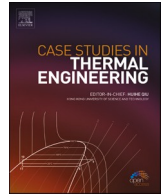




ELSEVIER

Contents lists available at ScienceDirect

## Case Studies in Thermal Engineering

journal homepage: [www.elsevier.com/locate/csite](http://www.elsevier.com/locate/csite)

# Magnetohydrodynamics squeeze flow of sodium alginate-based Jeffrey hybrid nanofluid with heat sink or source

Nur Azlina Mat Noor<sup>a</sup>, Sharidan Shafie<sup>b,\*</sup>

<sup>a</sup> School of Computing and Data Science, Xiamen University Malaysia, 43900, Sepang, Selangor Darul Ehsan, Malaysia

<sup>b</sup> Department of Mathematical Sciences, Faculty of Science, Universiti Teknologi Malaysia, 81310, Johor Bahru, Johor, Malaysia

## ARTICLE INFO

Handling Editor: Huihe Qiu

Keywords:

MHD

Jeffrey hybrid nanofluid

Sodium alginate

Squeezing flow

Chemical reaction

Heat source/sink

## ABSTRACT

The behavior of magnetohydrodynamics (MHD) flow, heat and mass transfer of Jeffrey hybrid nanofluid on the squeeze channel through permeable medium are discovered. The impacts of chemical reaction and heat sink/source are considered. The dimensionless equations are discretized by employing similarity transformation and Keller-box techniques. The dispersion of Copper ( $Cu$ ) and Alumina ( $Al_2O_3$ ) in the base fluid of sodium alginate ( $C_6H_9NaO_7$ ) are considered. The validation of the current outputs by comparing with existing outputs from reputable papers is conducted. The discussion on the velocity, temperature and concentration, and physical quantities of fluid are reviewed based on the graphical outputs with the effects of chemical reaction, Jeffrey fluid, magnetic, porous medium, nanoparticles volume fraction and heat sink/source. The graphical results shows the wall shear stress elevates for  $S$  and  $Ha$ , while it dropping for  $De$ ,  $\lambda_1$  and  $Da$ . The fluid velocity accelerates caused by squeezing of two surfaces, while it decelerates with increase in  $De$ ,  $Da$  and  $\varphi_2$  at the centre of channel. The resistance due to  $Ha$  and  $\lambda_1$  in the flow decrease the fluid velocity near the lower channel. The increment of convective heat transfer and temperature occurs with  $\gamma$  and  $Ec$  rises. The constructive chemical reaction and volume fraction of copper boosts the concentration and decrease the mass transfer rate of fluid flow, whereas adverse impact is discovered for destructive chemical reaction.

## Nomenclature

$B$	magnetic field
$C$	concentration of fluid
$C_w$	concentration at upper plate
$C_p$	specific heat ( $Jkg^{-1}K^{-1}$ )
$Ec$	Eckert Number
$De$	Deborah Number
$Da$	Darcy number
$h$	distance of two plates ( $m$ )
$Ha$	Hartmann number
$k_1^*$	mean absorption ( $m^{-1}$ )

\* Corresponding author.

E-mail address: [sharidan@utm.my](mailto:sharidan@utm.my) (S. Shafie).

<https://doi.org/10.1016/j.csite.2023.103303>

Received 21 February 2023; Received in revised form 10 July 2023; Accepted 14 July 2023

Available online 15 July 2023

2214-157X/© 2023 The Authors. Published by Elsevier Ltd. This is an open access article under the CC BY license (<http://creativecommons.org/licenses/by/4.0/>).

$k_c$	chemical reaction rate
$k_1$	permeability of porous medium
$k_{Al_2O_3}$	thermal conduction of alumina ( $Wm^{-1}K^{-1}$ )
$k_{Cu}$	thermal conduction of copper
$k_{hnf}$	thermal conduction of hybrid nanofluid
$k_f$	thermal conduction of sodium alginate
$l$	initial distance of two plates ( $m$ )
$\varphi_{Cu}/\varphi_2$	volume fraction of copper
$\varphi_{Al_2O_3}/\varphi_1$	volume fraction of alumina
$\varphi_{hnf}$	volume fraction of hybrid nanofluid
$(\rho C_p)_f$	heat capacity of sodium alginate
$(\rho C_p)_{Al_2O_3}$	heat capacity of alumina
$(\rho C_p)_{Cu}$	heat capacity of copper
$(\rho C_p)_{hnf}$	heat capacity of hybrid nanofluid
$Pr$	Prandtl number
$Q$	heat source/sink
$R$	chemical reaction parameter
$Sc$	Schmidt number
$S$	squeeze number
$t$	time ( $s$ )
$T$	temperature of fluid ( $K$ )
$T_w$	temperature at upper plate ( $K$ )
$u$	flow velocity in $x$ axis ( $ms^{-1}$ )
$v$	flow velocity in $y$ axis ( $ms^{-1}$ )
$v_w$	velocity at upper surface ( $ms^{-1}$ )
<b>Greek symbols</b>	
$\alpha_f$	thermal diffusion of Jeffrey fluid ( $Wm^2J^{-1}$ )
$\alpha$	constant
$f$	dimensionless velocity
$\theta$	dimensionless temperature
$\delta$	dimensionless length
$\gamma$	dimensionless heat source/sink
$\eta$	boundary layer thickness
$\varphi$	porosity of permeable medium
$\nu_f$	kinematic viscosity ( $m^2s^{-1}$ )
$\rho_f$	fluid density ( $kgm^{-3}$ )
$\rho_p$	density of nanoparticles
$\sigma_{Al_2O_3}$	electrical conduction of alumina ( $Sm^{-1}$ )
$\sigma_{Cu}$	electrical conduction of copper
$\sigma_{hnf}$	electrical conduction of hybrid nanofluid
$\sigma_f$	electrical conduction of sodium alginate
$\lambda_2$	retardation time
$\lambda_1$	ratio of relaxation and retardation times
$\varphi$	non-dimensional concentration

## 1. Introduction

The compression of fluid between two plates which caused the fluid starts to flow is known as squeezing flow. It has been studied by several scientists due to its utilization in geometry model of flow for lubricant in hydraulic lifts, injection moulding and bearings. The study of squeezing viscous flow through horizontal channel is proposed by Stefan [1]. Later, Cameron [2] explored the review of squeeze lubricant fluid past two infinite surfaces. The new similarity transformation is discovered by Wang [3] to simplify Navier-Stokes to ordinary differential equations for squeeze flow of viscous fluid. Then, the analytical solution was studied by Bujurke et al. [4], Rashidi et al. [5] and Khan et al. [6] based on Wang [3] research.

Jeffrey fluid has received great interest from scientist due to its display both relaxation and retardation properties. The behavior of the fluid depending on the imposed shear stress. It is classified as a shear thinning flow because it can be transformed to Newtonian fluid when the high force imposed on the fluid [7]. Pavlovskii [8] introduced the governing equation of Jeffrey fluid to explore the dynamic of aqueous polymer fluid. Based on the experimental study, the velocity of fluid decelerates by adding small volume of

polymers due to the increment of drag force in viscous fluid. Several researchers agreed that the rheology of Jeffrey fluid is suitable to be implemented for modelling of the blood flow across thin artery [9], flow of chyme in small intestine [10] and research on the aqueous Polyacrylamide fluid [11].

One of the significance mechanisms that affects the behavior of fluid is magnetohydrodynamics (MHD). The MHD exerted on the electrical conduction flow result in the production of Lorentz force. Common examples of the fluid are electrolytes, salt water and plasma [12]. The research on MHD was started with the invention of electromagnetic pump by Hartmann in 1918. Later, Hannes Alfven discovered a new type of plasma waves called Alfven waves and won Nobel prize for his contribution. It is classified as MHD waves because the Lorentz force induces the oscillation of ion in the plasma [13]. The application of MHD involving medical and engineering, in which it acts as a carrier for magnetic drug in body, mass spectrometers and cyclotrons [14]. Moreover, the flow in porous medium has gained interest among researchers as it can be applied in the analysis of oil extraction, geothermal energy recovery and porous burners. It is noted that velocity of the flow depends on the permeability and porosity of the medium [15]. The study of Jeffrey flow with magnetohydrodynamics (MHD) in permeable medium is addressed in several geometrical models. Hayat et al. [16] examined the influences of injection and suction on magneto-Jeffrey flow over squeezing permeable medium by applying homotopy analysis approach. Then, Hayat et al. [16] works is continued by Muhammad et al. [17] by studying the lower plate with influence of stretching porous plate. Nallapu and Radhakrishnamacharya [18] studied the MHD Jeffrey flow in permeable medium over circular channel. The hydromagnetic Jeffrey flow is explored by Ahmad and Ishak [19] at a stagnation point through stretched vertical surface numerically using Keller-box technique. Hayat et al. [20] analyzed the MHD Jeffrey nanofluid flow driven by squeeze of two disks.

The fluid flow with heat source or sink exhibit practical usages in industry such as metal formation, drawing of glass fibre and heat exchangers. The role of heat source and sink is to boost and reduce the thermal conductivities of fluid, respectively. The fluid with high conductivity raises the fluid temperature, whereas opposite behavior is shown for low conductivity fluid [21]. Qasim [22] discussed the influences of heat sink/source on the thermal and mass transfer on a horizontal stretched surface by power series technique. Ahmed et al., 2015 [23] reported the radiative heat transfer of MHD Jeffrey flow through a vertical stretched surface with heat sink/source, joule heating and dissipation. Mamatha et al. [24] explored the suction and heat sink/source impacts on hydromagnetic Jeffrey flow past a shrinking surface using shooting method. Avinash et al. [25] examined the heat transfer of Jeffrey nanofluid flow through stretched surface for the effects of non-uniform heat source/sink.

The influence of chemical reaction on mass transport is important in the chemical and hydrometallurgical industries. The transport processes caused by chemical reaction usually arise in the nuclear reactor safety and solar collectors. The investigation of chemical reaction for the various flow geometry is explored [26]. Muzara and Shateyi [27] discussed the impacts of chemical reaction on radiative thermal transfer of magneto-Jeffrey flow across vertical plate with heat sink/source and joule dissipation. Saleem et al. [28] analyzed the convective thermal and mass transfer of MHD Jeffrey flow over a rotation cone under thermophoresis, chemical reaction and heat sink/source effects. Noor et al. [29] examined the influences of heat sink/source and chemical reaction on MHD squeeze flow and radiative heat transfer of Jeffrey fluid in porous medium with joule dissipation and heating. The similar problem is conducted by Noor et al. [30] for the study of Jeffrey fluid with nanoparticles. Then, Noor et al. [31] extended the previous studies by considering Soret and Dufour impacts in the Jeffrey flow.

The advancement in the thermal exchanger applications such as cooling in refrigerator, air condition and automotive equipment not able to be adapted using conventional fluids [32]. It has poor thermal transfer efficiency due to low thermal conductivities. Therefore, an innovated working fluid, known as nanofluid was developed by Choi and Eastman [33] with the dispersion of metallic particles in the base fluid. Nanofluid is very applicable to improve the capability of heat transfer in fluid and energy consumption in the thermal devices. Nowadays, many scientists have conducted the research on a new advanced thermal transfer fluid, called hybrid nanofluid to boost the efficiency of thermal devices. It is made up of two or more nanoparticles with high thermal conductivities such as copper (Cu), silver (Ag) and gold (Au). Turcu et al. [34] and Jana et al. [35] conducted the experiments to analyse the features of hybrid nanoparticles. Later, the manufacture of hybrid nanofluid using thermochemical technique is carried out by Suresh et al. [36].

The implementation of hybrid nanofluid in the high technology applications, which function as coolant in electronic appliances, vehicle engines and nuclear power system have been acknowledged by several researchers [37]. They have discovered hybrid nanofluid flow in different geometries. For Casson hybrid nanofluid, Alghamdi et al. [38] investigated the MHD flow and thermal transfer at a stagnation point through horizontal stretching surface. Then, Abbas et al. [39] explored the nonlinear radiative thermal transfer on stagnation point flow with MHD, thermal slip and viscous dissipation effects at vertical stretched surface. The signal wall and multi-wall carbon nanotubes with conventional fluid is considered. Mahabaleswar et al. [40] studied the MHD flow and radiative thermal transfer of Cu-Al<sub>2</sub>O<sub>3</sub>/H<sub>2</sub>O hybrid nanofluid on porous stretch/shrink surface with velocity slip condition. Khashi'ie et al. [41] analyzed the impact of injection/suction on hydromagnetic squeeze flow of Cu-Al<sub>2</sub>O<sub>3</sub>/H<sub>2</sub>O hybrid nanofluid at lower stretching surface. Later, Famakinwa et al. [42] extended Khashi'ie et al. [41] work by examining the effects of variable viscosity on MHD flow and radiative thermal transfer of Cu-Al<sub>2</sub>O<sub>3</sub>/H<sub>2</sub>O fluid with joule dissipation. Jyothi et al. [43] discovered the heat sink/source impacts on squeeze flow, thermal and mass transfer of Casson hybrid nanofluid with thermophoresis. For Jeffrey hybrid nanofluid, Asjad et al. [44] reported the flow and thermal transfer of Jeffrey fluid with ternary nanoparticles through infinitely vertical surface using fractional model. Khan et al. [45] examined the MHD flow, radiative thermal and mass transfer across inclined oscillating surface in a permeable medium with slip effect by fractional model.

A literature survey shows that most of the researches are conducted on the squeeze Jeffrey flow over two plates. The mass and thermal transfer of MHD hybrid nanofluid by squeeze of two plates with chemical reaction effects has not yet been explored. Generally, limited research is explored on squeezing Jeffrey hybrid nanofluid flow. Therefore, this study investigates unsteady MHD squeeze flow of Jeffrey hybrid nanofluid through two plates saturated in porous medium. The mass and thermal transfer with the influences of chemical reaction and heat sink/source are examined. The hybrid nanoparticles of copper and alumina with the base fluid of sodium

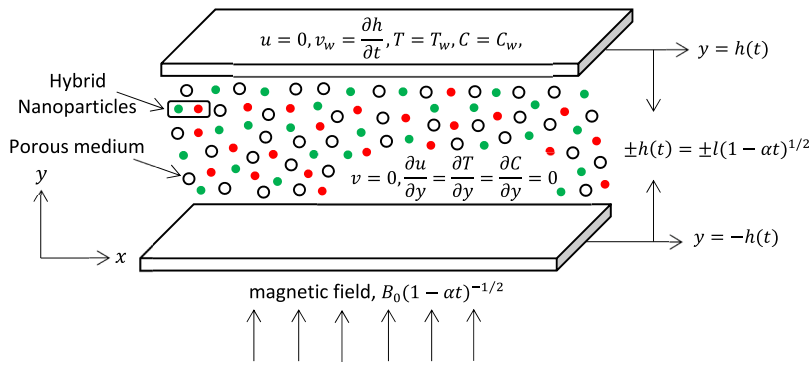


Fig. 1. Geometry model of squeeze flow of hybrid nanofluid.

Table 1  
Correlations of the thermophysical properties for hybrid nanofluid.

Properties	Hybrid nanofluid
Dynamic viscosity ( $\mu$ )	$\frac{\mu_{hnf}}{\mu_f} = \frac{1}{(1 - \varphi_{hnf})^{2.5}}$
Density ( $\rho$ )	$\rho_{hnf} = (1 - \varphi_{hnf})\rho_f + \varphi_{Al_2O_3}\rho_{Al_2O_3} + \varphi_{Cu}\rho_{Cu}$
Heat capacity ( $\rho C_p$ )	$(\rho C_p)_{hnf} = (1 - \varphi_{hnf})(\rho C_p)_f + \varphi_{Al_2O_3}(\rho C_p)_{Al_2O_3} + \varphi_{Cu}(\rho C_p)_{Cu}$
Electrical conductivity ( $\sigma$ )	$\frac{\sigma_{hnf}}{\sigma_f} = \left[ 1 + \frac{3\varphi_{hnf}(\varphi_{Al_2O_3}\sigma_{Al_2O_3} + \varphi_{Cu}\sigma_{Cu} - \sigma_f(\varphi_{Al_2O_3} + \varphi_{Cu}))}{\varphi_{Al_2O_3}\sigma_{Al_2O_3} + \varphi_{Cu}\sigma_{Cu} + 2\varphi_{hnf}\sigma_f - \varphi_{hnf}\sigma_f(\varphi_{Al_2O_3}\sigma_{Al_2O_3} + \varphi_{Cu}\sigma_{Cu} - \sigma_f(\varphi_{Al_2O_3} + \varphi_{Cu}))} \right]$
Thermal conductivity ( $k$ )	$\frac{k_{hnf}}{k_f} = \left[ \frac{\left( \frac{\varphi_{Al_2O_3}k_{Al_2O_3} + \varphi_{Cu}k_{Cu}}{\varphi_{hnf}} \right) + 2k_f + 2(\varphi_{Al_2O_3}k_{Al_2O_3} + \varphi_{Cu}k_{Cu}) - 2\varphi_{hnf}k_f}{\left( \frac{\varphi_{Al_2O_3}k_{Al_2O_3} + \varphi_{Cu}k_{Cu}}{\varphi_{hnf}} \right) + 2k_f - (\varphi_{Al_2O_3}k_{Al_2O_3} + \varphi_{Cu}k_{Cu}) + \varphi_{hnf}k_f} \right]$

Table 2  
Thermophysical properties for Copper, Alumina and Sodium Alginate.

Properties	Cu	Al <sub>2</sub> O <sub>3</sub>	Sodium alginate (C <sub>6</sub> H <sub>9</sub> NaO <sub>7</sub> )
$\rho$	8933	3970	989
$C_p$	385	765	4175
$\sigma$	$5.96 \times 10^7$	$3.69 \times 10^7$	0.07
$k$	400	40	0.6367
$Pr$	–	–	6.5

alginate are used in the experiment.

## 2. Mathematical formulation

The unsteady squeezing flow of Jeffrey hybrid nanofluid over two plates in permeable medium with MHD, chemical reaction and heat sink/source are investigated. The hybrid nanoparticles of copper and alumina with base fluid of sodium alginate are considered. The two surfaces are separated with distance  $y = \pm h(t) = \pm l(1 - \alpha t)^{\frac{1}{2}}$ . The external velocity  $v_w(t) = \frac{\partial h(t)}{\partial t}$  is imposed on upper and lower surfaces. The two surfaces are moves apart for  $\alpha < 0$  and the surfaces are moves closer for  $\alpha > 0$  until  $t = 1/\alpha$ . The bottom surface is exerted with magnetic field,  $B(t) = B_0(1 - \alpha t)^{-1/2}$  vertically [46]. Fig. 1 shows the geometry model of squeeze flow for hybrid nanofluid. The correlation and values of thermophysical properties for hybrid nanofluid is demonstrated in Table 1 and Table 2 [47].

The general form of continuity, momentum, energy and concentration equations of Jeffrey hybrid nanofluid in the vector notation are [48,49].

$$\frac{\partial \rho}{\partial t} + \nabla \cdot (\rho \mathbf{V}) = 0, \tag{1}$$

$$\rho_{hnf} \left( \frac{\partial \mathbf{V}}{\partial t} + (\mathbf{V} \cdot \nabla) \mathbf{V} \right) = \text{div } \mathbf{T} - \sigma_{hnf} [\mathbf{V} \times \mathbf{B}_1] \times \mathbf{B}_1 - \frac{\mu_{hnf} \varphi}{k_1} \mathbf{V}, \tag{2}$$

$$(\rho C_p)_{hnf} \left( \frac{\partial T}{\partial t} + (\mathbf{V} \cdot \nabla) T \right) = \text{Tr} (\mathbf{T} \cdot \mathbf{L}) - \nabla \cdot \mathbf{q}, \tag{3}$$

$$\frac{\partial C}{\partial t} + (\mathbf{V} \bullet \nabla)C = D_m \nabla^2 C - k_c C. \tag{4}$$

where  $\mathbf{J} \times \mathbf{B} = \sigma[\mathbf{V} \times \mathbf{B}_1] \times \mathbf{B}_1$  is the Lorentz force with  $\mathbf{B}_1$  transverse magnetic field is applied perpendicular to the plate. Based on Equation (2), left-hand side represents inertial forces, while the first term on right-hand side is surface force, second term is Lorentz force and third term is Darcy's resistance. For Equation (3), left-hand side represents total internal energy of the system, while the first term on right-hand side is due to viscous dissipation and second term for Fourier's law of heat conduction. For Equation (4), left-hand side represents total internal mass of the system, while the first term on right-hand side is molar flux due to diffusion and second term for convective total flux of chemical reaction. The Cauchy stress tensor  $\mathbf{T}$  for Jeffrey fluid is defined as

$$\mathbf{T} = -p\mathbf{I} + \mathbf{S}, \tag{5}$$

where  $p$  is the pressure and  $\mathbf{I}$  is the identity tensor. The definition of extra stress tensor  $\mathbf{S}$  is given by

$$\mathbf{S} = \frac{\mu}{1 + \lambda_1} \left( \mathbf{A}_1 + \lambda_2 \frac{d\mathbf{A}_1}{dt} \right), \tag{6}$$

where the Rivlin-Eriksen tensor  $\mathbf{A}_1$  is expressed as

$$\mathbf{A}_1 = \nabla \mathbf{V} + (\nabla \mathbf{V})^T. \tag{7}$$

The continuity, momentum, energy and mass equations are derived based on conservation law of mass, Newton's second law, first law of thermodynamics and principle of mass conservation, respectively. Then, the governing equations of Jeffrey hybrid nanofluid are reduced to the following equations using boundary layer approximation [27,43].

$$\frac{\partial u}{\partial x} + \frac{\partial v}{\partial y} = 0, \tag{8}$$

$$\frac{\partial u}{\partial t} + u \frac{\partial u}{\partial x} + v \frac{\partial u}{\partial y} = \frac{\mu_{hnf}}{\rho_{hnf}} \left( 1 + \frac{1}{\lambda_1} \right) \frac{\partial^2 u}{\partial y^2} + \frac{\mu_{hnf}}{\rho_{hnf}} \frac{\lambda_2}{1 + \lambda_1} \left( \frac{\partial^3 u}{\partial t \partial y^2} + u \frac{\partial^3 u}{\partial x \partial y^2} + v \frac{\partial^3 u}{\partial y^3} - \frac{\partial u}{\partial x} \frac{\partial^2 u}{\partial y^2} + \frac{\partial u}{\partial y} \frac{\partial^2 u}{\partial x \partial y} \right) - \frac{\sigma_{hnf} B(t)^2}{\rho_{hnf}} u - \frac{\mu_{hnf}}{\rho_{hnf}} \left( 1 + \frac{1}{\lambda_1} \right) \frac{\varphi}{k_1(t)} u, \tag{9}$$

$$\frac{\partial T}{\partial t} + u \frac{\partial T}{\partial x} + v \frac{\partial T}{\partial y} = \frac{k_{hnf}}{(\rho C_p)_{hnf}} \frac{\partial^2 T}{\partial y^2} + \frac{\mu_{hnf}}{(\rho C_p)_{hnf}} \left( 1 + \frac{1}{\lambda_1} \right) \left[ 4 \left( \frac{\partial u}{\partial x} \right)^2 + \left( \frac{\partial u}{\partial y} \right)^2 \right] - \frac{Q(t)}{(\rho C_p)_{hnf}} T, \tag{10}$$

$$\frac{\partial C}{\partial t} + u \frac{\partial C}{\partial x} + v \frac{\partial C}{\partial y} = D_m \frac{\partial^2 C}{\partial y^2} - k_c(t) C. \tag{11}$$

The correlated boundary conditions are

$$u = 0, v = v_w = \frac{\partial h(t)}{\partial t}, T = T_w, C = C_w, \text{ at } y = h(t), \tag{12}$$

$$\frac{\partial u}{\partial y} = 0, \frac{\partial^3 u}{\partial y^3} = 0, v = 0, \frac{\partial T}{\partial y} = 0, \frac{\partial C}{\partial y} = 0, \text{ at } y = 0. \tag{13}$$

The simplification of partial differential equations (PDEs) to ordinary differential equations (ODEs) are discretized by employing the following non-dimensional variables [50];

$$u = \frac{\alpha x}{2(1 - \alpha t)} f'(\eta), v = -\frac{\alpha l}{2\sqrt{(1 - \alpha t)}} f(\eta), \eta = \frac{y}{l\sqrt{(1 - \alpha t)}}, \theta = \frac{T}{T_w}, \varphi = \frac{C}{C_w}, \tag{14}$$

Substitute the similarity variables (14) into equations (9)–(11), the non-dimensional ODE forms are

$$\frac{\mu_{hnf}}{\mu_f} \frac{\rho_f}{\rho_{hnf}} \left( 1 + \frac{1}{\lambda_1} \right) f^{iv} - S(\eta f''' + 3f'' + f' f'' - f f''') + \frac{\mu_{hnf}}{\mu_f} \frac{\rho_f}{\rho_{hnf}} \left( 1 + \frac{1}{\lambda_1} \right) \frac{De}{2} (\eta f^{iv} + 5f^{iv} + 2f'' f''' - f' f^{iv} - f f^{iv}) \tag{15}$$

$$-\frac{\sigma_{hnf}}{\sigma_f} \frac{\rho_f}{\rho_{hnf}} Ha^2 f'' - \frac{\mu_{hnf}}{\mu_f} \frac{\rho_f}{\rho_{hnf}} \left( 1 + \frac{1}{\lambda_1} \right) \frac{1}{Da} f'' = 0,$$

$$\frac{(\rho C_p)_f}{(\rho C_p)_{hnf}} \frac{k_{hnf}}{k_f} \frac{1}{Pr} \theta'' + S(f\theta' - \eta\theta') + \frac{(\rho C_p)_f}{(\rho C_p)_{hnf}} \gamma\theta + \frac{\mu_{hnf}}{\mu_f} \frac{(\rho C_p)_f}{(\rho C_p)_{hnf}} Ec \left[ \left( 1 + \frac{1}{\lambda_1} \right) [(f'')^2 + 4\delta^2 (f')^2] \right] = 0, \tag{16}$$

$$\frac{1}{Sc} \varphi'' + S(f\varphi' - \eta\varphi') - R\varphi = 0. \tag{17}$$

**Table 3**  
 Numerical results of  $-f''(1)$  for  $S$  with  $\lambda_1 \rightarrow \infty, Da \rightarrow \infty, De \rightarrow \infty, Ha = Ec = \delta = \gamma = R = \varphi_2 = 0$  and  $Sc = Pr = 1$ .

$S$	Naduvanamani and Shankar [52]	Jyothi et al. [43]	Present outputs
-1.0	2.170090	2.170090	2.170255
-0.5	2.617403	2.617403	2.617512
0.01	3.007133	3.007133	3.007208
0.5	3.336449	3.336449	3.336504
2.0	4.167389	4.167389	4.167411

The corresponded boundary conditions.

$$f(\eta) = 0, f''(\eta) = 0, f^{iv}(\eta) = 0, \theta'(\eta) = 0, \varphi'(\eta) = 0, \text{ at } \eta = 0, \tag{18}$$

$$f(\eta) = 1, f'(\eta) = 0, \theta(\eta) = 1, \varphi(\eta) = 1, \text{ at } \eta = 1. \tag{19}$$

The significant terms in the governing equations are defined as

$$S = \frac{\alpha l^2}{2\nu_f}, Ha = lB_0 \sqrt{\frac{\sigma}{\rho_f \nu_f}}, De = \frac{\alpha \lambda_2}{1 - \alpha t}, Da = \frac{k_0}{\varphi l^2}, \delta = \frac{l}{x}(1 - \alpha t)^{1/2}, Pr = \frac{\nu_f}{\alpha_f}, Ec = \frac{\alpha^2 x^2}{4C_p T_w (1 - \alpha t)^2},$$

$$\gamma = \frac{Q_0 l^2}{\nu_f (\rho C_p)_f}, Sc = \frac{\nu_f}{D_m}, R = \frac{ak_2 l^2}{\nu_f}.$$

**3. Results and discussion**

The computation of the ordinary differential equations (15)–(17) with boundary conditions (18) and (19) are calculated by implementing Keller-box approaches. The solutions are executed numerically and graphically through MATLAB software. The accurate results are obtained using proper step size,  $\Delta\eta = 0.01$  and boundary layer thickness,  $\eta_\infty = 1$ . The calculation using algorithm in MATLAB is stopped when the difference of current and previous results for velocity, temperature, and concentration converges to  $10^{-5}$  [51].

The investigation on the effect of  $S, Da, \lambda_1, Ha, De, \varphi_2, Ec, \gamma, R$  and  $Sc$  are done to examine the behavior of velocity, temperature, and concentration. The validation of the current outputs obtained from Keller-box techniques is conducted by comparing the skin friction coefficient with Naduvanamani and Shankar [52] and Jyothi et al. [43] in Table 3 as limiting cases.

The graphical outputs for influences of  $S, \lambda_1, Ha, De, Da$  and  $\varphi_2$  on velocity of fluid are shown in Fig. 2(a) to 2(f). The movement of

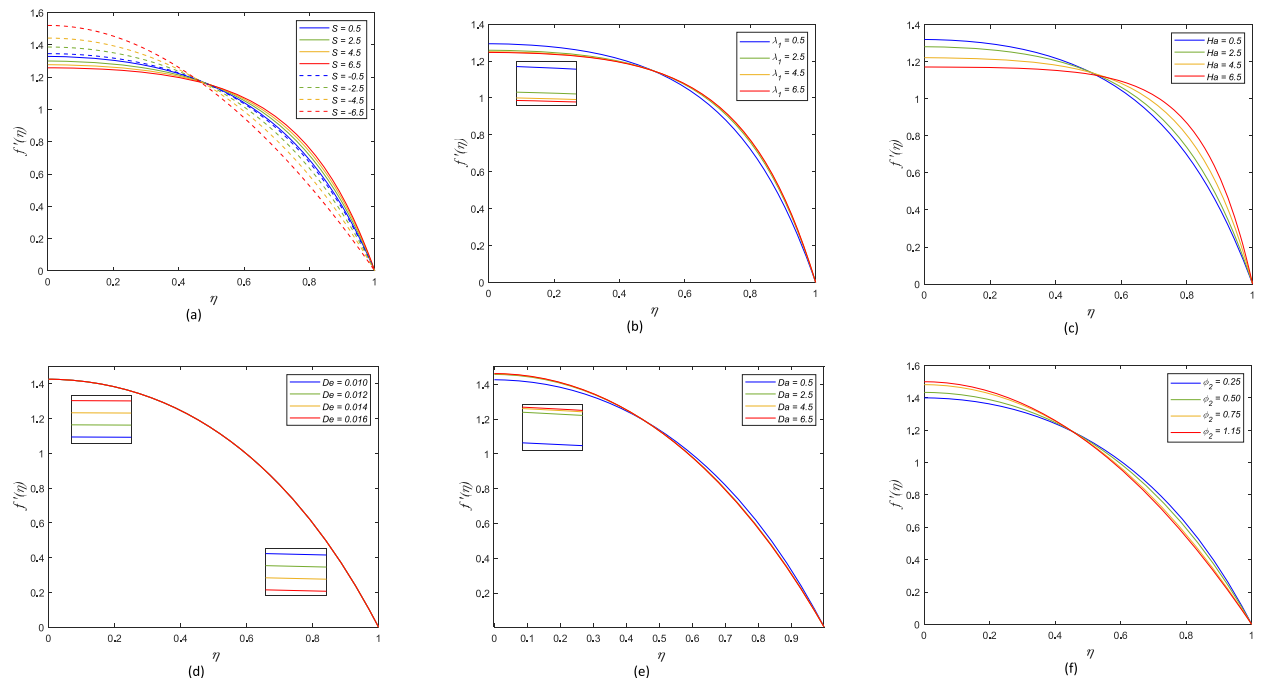


**Fig. 2.** Influences of (a)  $S$ , (b)  $\lambda_1$ , (c)  $Ha$ , (d)  $De$ , (e)  $Da$  and (f)  $\varphi_2$  on  $f'(\eta)$ .

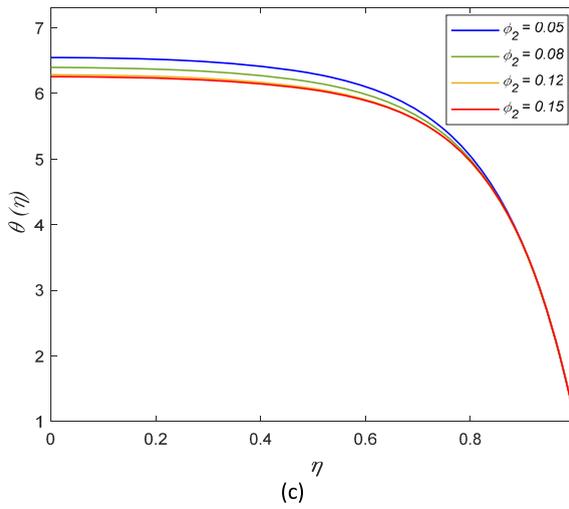
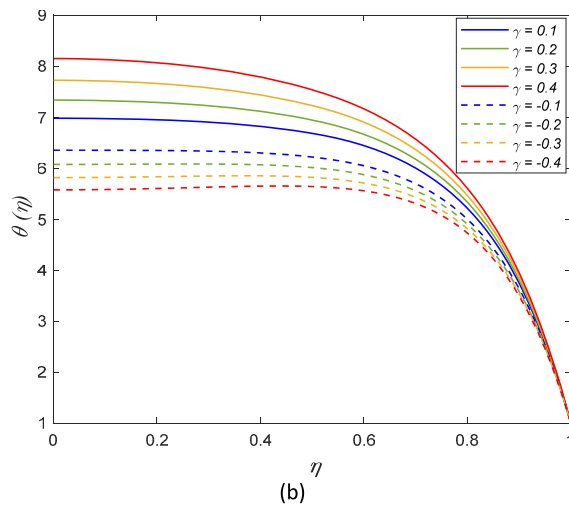
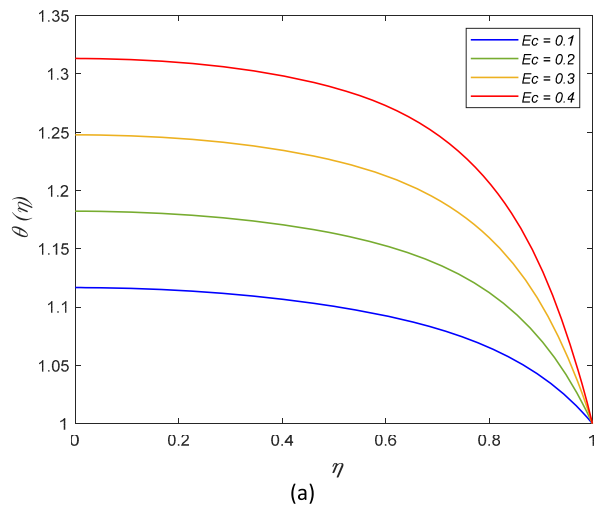


Fig. 3. Influences of (a)  $Ec$ , (b)  $\gamma$  and (c)  $\phi_2$  on  $\theta(\eta)$ .

two surfaces is denoted by squeezing parameter,  $S$ . The surfaces moving nearer with  $S > 0$ , while the surfaces moving further with  $S < 0$ . Fig. 2(a) displays the velocity of fluid decelerates at the region nearby lower surfaces,  $\eta < 0.45$ , whereas it accelerates at the region far from surfaces,  $\eta \geq 0.45$  for  $S > 0$ . On the contrary, the velocity rises at  $\eta < 0.45$ , whereas it decreasing at  $\eta \geq 0.45$  for  $S < 0$ . Based on the physical interpretation, the fluid flow pass across the thin channel rapidly due to the compression of the surfaces, whereas the velocity slowing down because the flow opposes high resistancy in the broader channel. Fig. 2(b) exhibits the axial velocity declines at  $\eta < 0.5$ , whereas it enhances at  $\eta > 0.5$  when  $\lambda_1$  increasing. It is noticed the addition of  $\lambda_1$  raise the intermolecular forces of particles, which cause the flow viscosity increases and velocity drops near the lower plate. Fig. 2(c) portrays the velocity declining at  $\eta \leq 0.5$ , whereas it enhancing for  $\eta > 0.5$  with rising  $Ha$ . It is shown that the magnetic field exerted on the lower surface causes the velocity of fluid slowing down. The Lorentz force produced by MHD increase the resistancy on the flow. Fig. 2(d) presents the velocity escalates nearer the upper surface, whereas it declines nearer the lower surface for elevating  $De$ . Deborah parameter is the ratio of retardation time and observation time. The retardation time implies the slow response occurs when stress is imposed on the fluid. It is noted the fluid exhibits high retardation time because the flow viscosity boosts as the intermolecular forces of particles become stronger with enhancement of  $De$ . This phenomenon slowing down the velocity of flow at centre of two plates. Fig. 2(e) depicts the velocity elevating at  $\eta \leq 0.5$ , whereas it decelerating at  $\eta > 0.5$  with rises  $Da$ . The addition of Darcy number implies the higher permeability of medium, and hence boost the flow across the region. Fig. 2(f) shows the velocity increasing at  $\eta \leq 0.5$  and it drops at  $\eta > 0.5$  for elevating  $\phi_2$ . The reduction of velocity at centre of channel when nanoparticles rise is due to the fluid not able to flow smoothly caused by the stronger collision between fluid particles and nanoparticles.

The influences of  $Ec$ ,  $\gamma$  and  $\phi_2$  on temperature of fluid flow are demonstrated in Fig. 3(a) and (b) and 3(c). Fig. 3(a) shows the temperature escalates when the heat produced by the movement of flow particles in the high viscosity of fluid boosts. It has resulted in enhancement of kinetic energy in the particles when  $Ec$  increases. Fig. 3(b) illustrates the temperature reduces for increasing heat sink ( $\gamma < 0$ ), whereas it escalates for increasing heat source ( $\gamma > 0$ ). High heat sink implies the thermal energy transfer from fluid to the surfaces boosts, which causes the temperature drop in the flow. Meanwhile, the increment of heat sink promotes the thermal energy in

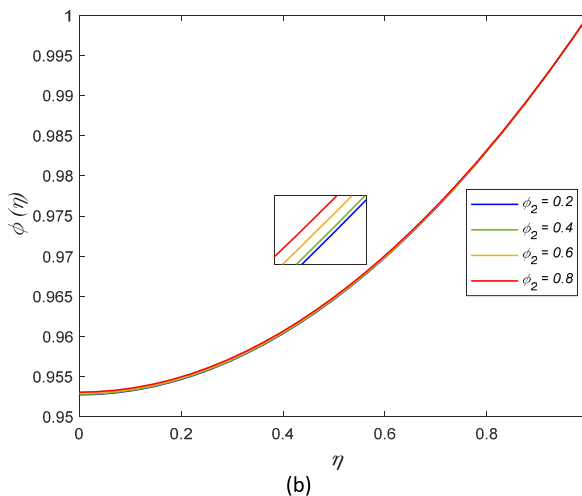
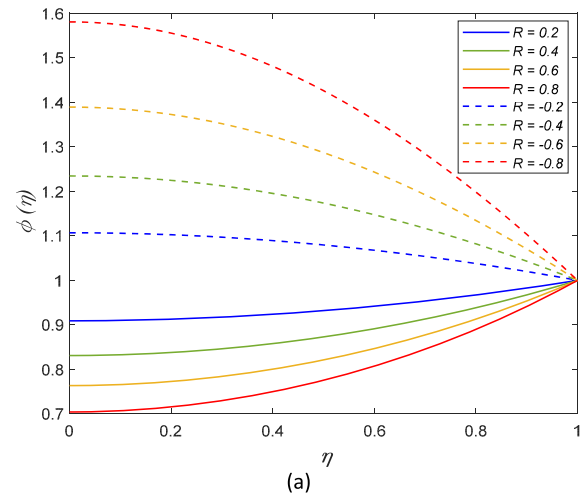


Fig. 4. Influences of (a)  $R$  and (b)  $\phi_2$  on  $\phi(\eta)$ .

the flow region and thus, it accelerates the flow temperature. Fig. 3(c) displays the temperature decreases with raise in  $\varphi_2$ . The reason is the nanoparticle volume fraction promotes the kinetic energy and thermal conductivity in fluid. Hence, it enhances the rate of thermal transfer from fluid flow to plates, which cause the fluid temperature drops.

The influences of  $R$  and  $\varphi_2$  on concentration are demonstrated in Fig. 4(a) and (b). Fig. 4(a) depicts the concentration decreasing when destructive chemical reaction,  $R > 0$ , whereas it boosting when constructive chemical reaction,  $R < 0$ . The rate of chemical reaction boosts with raise in constructive reaction, while adverse impact is found in destructive reaction. Fig. 4(b) portrays the concentration rises for elevating  $\varphi_2$  because the high volume fraction of nanoparticles escalates the viscosity of fluid.

The influences of  $Ha$  and  $Da$  on wall shear stress are presented in Fig. 5. The shear stress at the wall increasing with raise in  $Ha$ , whereas it drops as  $Da$  rises. The reason is the induction of Lorentz force in fluid flow boosts for elevating  $Ha$  and thus, it strengthens the friction force nearby the surface wall. On the contrary, the fluid nearby wall moves rapidly when the permeability of porous medium increases. It indicates that the friction force in the fluid become weaker, which cause the shear stress decelerates at the boundary region. Fig. 6 displays the Nusselt number boost when  $Ec$  increases, while it decreases when  $R_d$  enhances. Nusselt number is denoted by the ratio of convective and conductive heat transfer. The increment of  $Ec$  raise the temperature of flow. The higher  $Ec$  indicates that the heat caused by motion of nanoparticles regulated the fluid temperature. Hence, it shows that the heat convection is more significant than conduction, which resulting in the enhancement of convective heat transfer and Nusselt number. Moreover, the rate of heat transfer escalates because of high temperature of fluid accelerates the kinetic energy in the flow as  $\gamma$  rises. The convective heat transfer in fluid increases and consequently, raise the Nusselt coefficient. Fig. 7 exhibits the Sherwood number escalates for  $R > 0$ , whereas it reduces for  $R < 0$  with rising  $Sc$ . Sherwood number is the ratio of convective and diffusive thermal transfer. The constructive reaction raise the high concentration in fluid, which enhancing the diffusive mass transfer. It implies that the Sherwood number and convective mass transfer declines in the fluid region. The adverse behaviour is observed for destructive chemical reaction due to the low fluid concentration cause the mass convection in fluid become more dominant and thus, boost the Sherwood number.

The fluid with hybrid nanoparticles is significance as a coolant in the radiator. The large radiator is used to maximize the cooling effects on the engine, which cause high energy is required to maintain the system. Hence, the implementation of hybrid nanofluid is potentially useful in the modelling of small size of radiator and it has presented a good outcome in energy saving and emission reduction [53]. Furthermore, the influence of magnetic field and porous medium is examined in the flow. It is discovered that the conversion of kinetic energy of particles into a voltage enhances by applying magnetic field and plasma conductivity [54]. The presence of chemical reaction in the mathematical model is to investigate the coolant in a nuclear reactor. It is used to remove heat from the nuclear reactor engine and transfer the heat to electrical generators and the environment [55].

Based on the results an, the high strength of magnetic field and permeability of porous medium should be considered in the flow of squeezing plates to increase the wall shear stress of fluid. It boosts the transformation of kinetic energy into a power voltage. The viscosity of fluid needs to be reduced by lowering the Jeffrey parameter. Moreover, the low heat and viscous dissipation parameter, while high nanoparticles volume fraction are considered to maintain and cooling the temperature of engine. Besides, the presence of

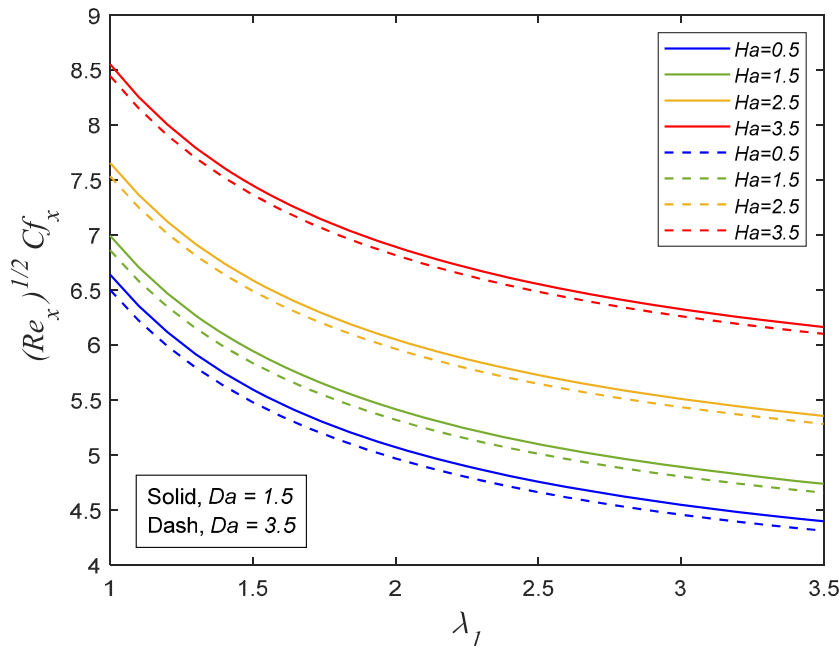


Fig. 5. Effect of  $\lambda_1$ ,  $Ha$  and  $Da$  on  $(Re_x)^{1/2}C_{f_x}$ .

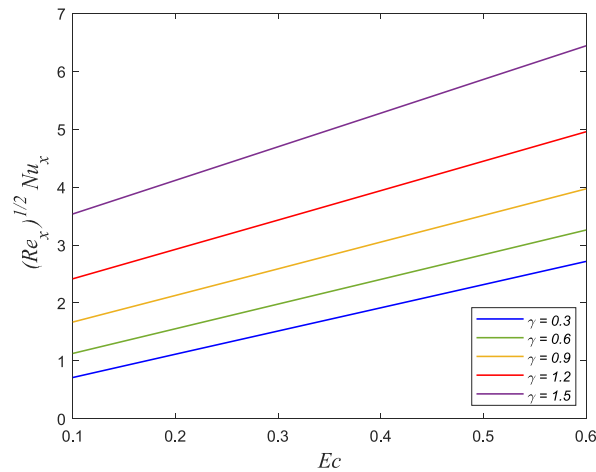


Fig. 6. Effect of  $Ec$  and  $\gamma$  on  $(Re_x)^{1/2}Nu_x$ .

constructive reaction is useful for the removal of heat from engine [56,57].

#### 4. Conclusions

The influences of chemical reaction and heat sink/source on unsteady MHD squeeze flow, thermal and mass transfer of Jeffrey hybrid nanofluid in a porous channel was examined. The numerical and graphical outputs is computed by employing Keller-box techniques and MATLAB programming. Validation of the current outputs with existing outputs from reputable papers is carried out. Physically, the impacts of  $S, Da, \lambda_1, Ha, De, \varphi_2, Ec, \gamma, R$  and  $Sc$  on velocity, temperature and concentration, and physical quantities on the fluid flow are analyzed. The significant results of Jeffrey hybrid nanofluid based on the discussion are deduced as:

1. The wall shear stress boosts with rises of  $S$  and  $Ha$ , in contrast it reduces with enhancing  $\lambda_1, De$  and  $Da$ .
2. The axial velocity accelerates once the surfaces is squeezed ( $S > 0$ ) and it decelerates once the surfaces is separated ( $S < 0$ ) at the middle of channel.
3. The axial velocity nearby the lower channel declines due to the increment of  $\lambda_1$  and  $Ha$ .
4. The deceleration of axial velocity of fluid is shown at the centre of channel when  $De, Da$  and  $\varphi_2$  enhances.
5. The temperature and convective heat transfer of fluid escalating as  $\gamma$  and  $Ec$  elevates, while adverse impact is noticed for increasing  $\varphi_2$ .
6. The concentration of fluid rises, whereas the convective mass transfer declines for  $R < 0$ . The opposite behavior of fluid is noticed for  $R > 0$ .

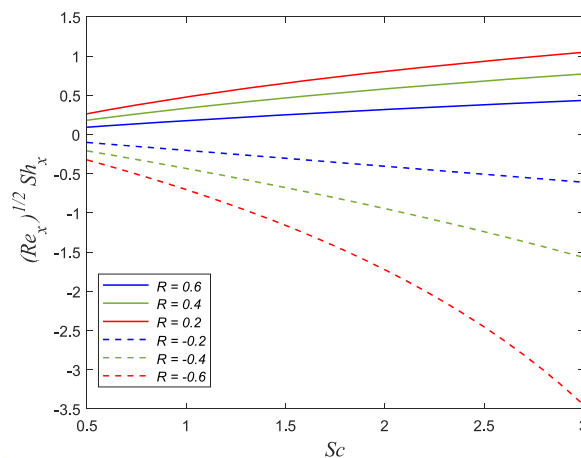


Fig. 7. Effect of  $Sc$  and  $R$  on  $(Re_x)^{1/2}Sh_x$ .

## Authorship statement

### Category 1

Conception and design of study:

Nur Azlina Mat Noor

acquisition of data: Nur Azlina Mat Noor

analysis and/or interpretation of data: Nur Azlina Mat Noor, Sharidan Shafie.

### Category 2

Drafting the manuscript: Nur Azlina Mat Noor, Sharidan Shafie

revising the manuscript critically for important intellectual content: Nur Azlina Mat Noor, Sharidan Shafie.

### Category 3

Approval of the version of the manuscript to be published (the names of all authors must be listed):

Nur Azlina Mat Noor, Sharidan Shafie

## Declaration of competing interest

The authors declare that they have no known competing financial interests or personal relationships that could have appeared to influence the work reported in this paper.

## Data availability

No data was used for the research described in the article.

## Acknowledgments

The authors would like to acknowledge the financial support from Universiti Teknologi Malaysia for the funding under UTM High Impact Research (UTMHR: Q.J130000.2454.08G33).

## References

- [1] M. Stefan, Experiments on apparent adhesion, the London, Edinburgh, and Dublin, Philosoph. Magazine J. Sci. 47 (314) (1874) 465–466.
- [2] A. Cameron, Basic Lubrication Theory, Prentice Hall Europe, 1981.
- [3] C.Y. Wang, The squeezing of a fluid between two plates, J. Appl. Mech. 43 (4) (1976) 579–583.
- [4] N.M. Bujurke, P.K. Achar, N.P. Pai, Computer extended series for squeezing flow between plates, Fluid Dynam. Res. 16 (1995) 173–187.
- [5] M. Rashidi, H. Shahmohamadi, S. Dinarvand, Analytic Approximate Solutions for Unsteady Two-Dimensional and Axisymmetric Squeezing Flows between Parallel Plates, Mathematical Problems in Engineering, 2008.
- [6] U. Khan, N. Ahmed, S.I. Khan, Z.A. Zaidi, Y. Xiao-Jun, S.T. Mohyud-Din, On unsteady two-dimensional and axisymmetric squeezing flow between parallel plates, Alex. Eng. J. 53 (2014) 463–468.
- [7] N.A.M. Noor, S. Shafie, M.A. Admon, MHD squeezing flow of Casson nanofluid with chemical reaction, thermal radiation and heat generation/absorption, Adv. Res. Fluid Mech. Thermal Sci. 68 (2) (2020) 94–111.
- [8] V.A. Pavlovskii, On theoretical description of weak aqueous solutions of polymers, Dokl. Akad. Nauk SSSR 200 (1971) 809–812.
- [9] N.S. Akbar, S. Nadeem, M. Ali, Jeffrey fluid model for blood flow through a tapered artery with a stenosis, J. Mech. Med. Biol. 11 (2011) 529–545.
- [10] N.S. Akbar, S. Nadeem, C. Lee, Characteristics of Jeffrey fluid model for peristaltic flow of chyme in small intestine with magnetic field, Results Phys. 3 (2013) 152–160.
- [11] S. Hamza, Modelling the effect of concentration on non-Newtonian apparent viscosity of an aqueous Polyacrylamide solution, Global J. Phys. 5 (2016) 505–517.
- [12] M. Sheikholeslami, D.D. Ganji, External Magnetic Field Effects on Hydrothermal Treatment of Nanofluid, first ed., Elsevier Science, United Kingdom, 2016.
- [13] P.A. Davidson, An Introduction to Magnetohydrodynamics, University Press, Cambridge, 2001.
- [14] E. D'Emili, L. Giuliani, A. Lisi, M. Ledda, S. Grimaldi, L. Montagnier, A.R. Libof, Lorentz force in water: evidence that hydronium cyclotron resonance enhances polymorphism, Electromagn. Biol. Med. 34 (4) (2014) 1–6.
- [15] S. Ahmad, M. Farooq, A. Anjum, N.A. Mir, Squeezing flow of convectively heated fluid in porous medium with binary chemical reaction and activation energy, Adv. Mech. Eng. 11 (2019) 1–12.
- [16] T. Hayat, R. Sajjad, S. Asghar, Series Solution for MHD Channel Flow of a Jeffrey Fluid, Communications in Nonlinear Science and Numerical Simulation, 2010.
- [17] T. Muhammad, T. Hayat, A. Alsaedi, A. Qayyum, Hydromagnetic unsteady squeezing flow of Jeffrey fluid between two parallel plates, Chin. J. Phys. 55 (2017) 1511–1522.
- [18] S. Nallapu, G. Radhakrishnamacharya, Jeffrey fluid flow through porous medium in the presence of magnetic field in narrow tubes, Int. J. Eng. Math. (2014).
- [19] K. Ahmad, A. Ishak, Magnetohydrodynamic flow and heat transfer of a Jeffrey fluid towards a stretching vertical surface, Therm. Sci. (2015).
- [20] T. Hayat, Z. Iqbal, M. Mustafa, A. Alsaedi, Unsteady flow and heat transfer of Jeffrey fluid over a stretching sheet, Therm. Sci. 18 (2014) 1069–1078.
- [21] N.A.M. Noor, S. Shafie, M.A. Admon, Heat and mass transfer on MHD squeezing flow of Jeffrey nanofluid in horizontal channel through permeable medium, PLoS One 16 (5) (2021), e0250402.
- [22] M. Qasim, Heat and mass transfer in a Jeffrey fluid over a stretching sheet with heat source/sink, Alex. Eng. J. 52 (2013) 571–575.
- [23] J. Ahmed, A. Shahzad, M. Khan, R. Ali, A note on convective heat transfer of an MHD Jeffrey fluid over a stretching sheet, AIP Adv. 5 (2015) 1–12.
- [24] S.U. Mamatha, M.K. Murthy, C.S.K. Raju, M.M. Hoque, Heat transfer effects on MHD flow of Jeffrey fluid over a shrinking sheet with heat source/sink and mass suction, Int. J. Renew. Sustain. Energy (2018) 85–93.
- [25] K. Avinash, N. Sandeep, O.D. Makinde, Non-uniform heat source/sink effect on liquid Film flow of Jeffrey nanofluid over a stretching sheet, Diffus. Found. 11 (2017) 72–83.
- [26] N.A.M. Noor, S. Shafie, M.A. Admon, Slip effects on MHD squeezing flow of Jeffrey nanofluid in horizontal channel with chemical reaction, Mathematics 9 (11) (2021) 1215.
- [27] H. Muzara, S. Shateyi, Analytical and numerical solutions of squeezing unsteady Cu and TiO<sub>2</sub>-nanofluid flow in the presence of thermal radiation and heat generation/absorption, Mathematics 9 (2021) 1896.
- [28] S. Saleem, M.M. Al-Qarni, S. Nadeem, N. Sandeep, Convective heat and mass transfer in magneto Jeffrey fluid flow on a rotating cone with heat source and chemical reaction, Commun. Theor. Phys. 70 (2018) 534–540.
- [29] N.A.M. Noor, S. Shafie, M.A. Admon, Unsteady MHD squeezing flow of Jeffrey fluid in a porous medium with thermal radiation, heat generation/absorption and chemical reaction, Phys. Scripta 95 (2020) 1–13.

- [30] N.A.M. Noor, S. Shafie, M.A. Admon, Impacts of chemical reaction on squeeze flow of MHD Jeffrey fluid in horizontal porous channel with slip condition, *Phys. Scripta* 96 (2021) 1–18.
- [31] N.A.M. Noor, S. Shafie, M.A. Admon, Soret and Dufour impacts on MHD squeeze flow of Jeffrey fluid in horizontal channel with thermal radiation, *PLoS One* 17 (5) (2022), e0266494.
- [32] N.A.M. Noor, S. Shafie, M.A. Admon, Effects of viscous dissipation and chemical reaction on MHD squeezing flow of Casson nanofluid between parallel plates in a porous medium with slip boundary condition, *Eur. Phys. J. Plus* 135 (2020).
- [33] S.U.S. Choi, J.A. Eastman, Enhancing thermal conductivity of fluids with nanoparticles, in: *Proceedings of the 1995 International Mechanical Engineering Congress and Exhibition, FED*, 1995, pp. 99–106.
- [34] R. Turcu, A. Darabont, A. Nan, N. Aldea, D. Macovei, D. Bica, L. Vekas, O. Pana, M.L. Soran, A.A. Koos, New polypyrrole-multiwall carbon nanotubes hybrid materials, *J. Optoelectron. Adv. Mater.* 8 (2006) 643–647.
- [35] S. Jana, A. Salehi-Khojin, W.H. Zhong, Enhancement of fluid thermal conductivity by the addition of single and hybrid nano-additives, *Thermochim. Acta* 462 (2007) 45–55.
- [36] S. Suresh, K.P. Venkataraj, P. Selvakumar, M. Chandrasekar, Synthesis of  $\text{Al}_2\text{O}_3\text{-Cu}$ /water hybrid nanofluids using two step method and its thermo physical properties, *Colloids Surfaces A Physicochem. Eng. Asp.* 388 (2011) 41–48.
- [37] N. Ahmed, F. Saba, U. Khan, I. Khan, T.A. Alkanhal, I. Faisal, S.T. Mohyud-Din, Spherical shaped ( $\text{Ag} - \text{Fe}_3\text{O}_4/\text{H}_2\text{O}$ ) hybrid nanofluid flow squeezed between two rigid plates with nonlinear thermal radiation and chemical reaction effects, *Energies* 12 (76) (2019).
- [38] W. Alghamdi, T. Gul, M. Nullah, A. Rehman, S. Nasir, A. Saeed, E. Bonyah, Boundary layer stagnation point flow of the Casson hybrid nanofluid over an unsteady stretching surface, *AIP Adv.* 11 (2021).
- [39] N. Abbas, W. Shatanawi, K. Abodayeh, Computational analysis of MHD nonlinear radiation Casson hybrid nanofluid flow at vertical stretching sheet, *Symmetry* 14 (2022) 1494.
- [40] U.S. Mahabaleshwar, H.A. Emad, T. Anusha, MHD slip flow of a Casson hybrid nanofluid over a stretching/shrinking sheet with thermal radiation, *Chin. J. Phys.* 80 (2022) 74–106.
- [41] N.S. Khashi'ie, I. Waini, N.M. Arifin, I. Pop, Unsteady squeezing flow of  $\text{Cu Al}_2\text{O}_3$ /water hybrid nanofluid in a horizontal channel with magnetic field, *Sci. Rep.* 11 (2021), 14128.
- [42] O.A. Famakinwa, O.K. Koriko, K.S. Adegbe, Effects of viscous dissipation and thermal radiation on time dependent incompressible squeezing flow of  $\text{CuO} - \text{Al}_2\text{O}_3$ /water hybrid nanofluid between two parallel plates with variable viscosity, *J. Comput. Math. Data Sci.* 5 (2022), 100062.
- [43] A.M. Jyothi, R.S.V. Kumar, J.K. Madhukesh, B.C. Prasannakumara, G.K. Ramesh, Squeezing flow of Casson hybrid nanofluid between parallel plates with a heat source or sink and thermophoretic particle deposition, *Heat Transfer* (2021).
- [44] M.I. Asjad, A. Riaz, A.S. Alnahdi, S.M. Eldin, New solutions of fractional Jeffrey fluid with ternary nanoparticles approach, *Micromachines* 13 (2022) 1963.
- [45] S.U. Khan, Usman, A. Raza, A. Kanwal, K. Javid, Mixed Convection Radiated Flow of Jeffrey-type Hybrid Nanofluid Due to Inclined Oscillating Surface with Slip Effects: a Comparative Fractional Model, *Waves Random Complex Media*, 2022, pp. 1–22.
- [46] N.A.M. Noor, S. Shafie, M.A. Admon, Unsteady MHD flow of Casson nanofluid with chemical reaction, thermal radiation and heat generation/absorption, *MATEMATIKA* 35 (2019) 33–52.
- [47] R. Ali, Y.A. Musawa, A. Qasim, A. Ul Haq, K. Al-Khaled, I.E. Sarris, Solution of water and sodium alginate-based Casson type hybrid nanofluid with slip and sinusoidal heat conditions: a prabhakar fractional derivative approach, *Symmetry* 14 (2022) 2658.
- [48] K. Muhammad, T. Hayat, A. Alsaedi, B. Ahmed, A Comparative Study for Convective Flow of Base Fluid (Gasoline Oil), Nanomaterial (SWCNTs) and Hybrid Nanomaterial (SWCNTs+MWCNTs), *Applied Nanoscience*, 2020.
- [49] K. Muhammad, T. Hayat, A. Alsaedi, OHAM Analysis of Fourth-Grade Nanomaterial in the Presence of Stagnation Point and Convective Heat-Mass Conditions, *Waves in Random and Complex Media*, 2021.
- [50] H.F. Oztop, E. Abu-Nada, Numerical study of natural convection in partially heated rectangular enclosures filled with nanofluids, *Int. J. Heat Fluid Flow* 29 (2008) 1326–1336.
- [51] N.A.M. Noor, S. Shafie, M.A. Admon, Heat transfer on MHD squeezing flow of Jeffrey fluid through porous medium with slip condition, *J. Nanofluids* 11 (1) (2022) 31–38.
- [52] N.B. Naduvinamani, U. Shankar, Thermal-diffusion and diffusion-thermo effects on squeezing flow of unsteady magnetohydrodynamic Casson fluid between two parallel plates with thermal radiation, *Sadhana* 44 (8) (2019).
- [53] M.V. Krishna, A.J. Chamkha, Hall and ion slip effects on MHD rotating boundary layer flow of nanofluid past an infinite vertical plate embedded in a porous medium, *Results Phys.* 15 (2019), 102652.
- [54] M.V. Krishna, A.J. Chamkha, Hall and ion slip effects on magnetohydrodynamic convective rotating flow of Jeffreys fluid over an impulsively moving vertical plate embedded in a saturated porous medium with Ramped wall temperature, *Numer. Methods Part. Differ. Equ.* 37 (3) (2020) 2150–2177.
- [55] M.V. Krishna, Numerical investigation on steady natural convective flow past a perpendicular wavy surface with heat absorption/generation, *Int. Commun. Heat Mass Tran.* 139 (2022), 106517.
- [56] M.V. Krishna, Hall and ion slip impacts on unsteady MHD free convective rotating flow of Jeffreys fluid with ramped wall temperature, *Int. Commun. Heat Mass Tran.* 119 (2020), 104927.
- [57] M.V. Krishna, Hall and ion slip effects on radiative MHD rotating flow of Jeffreys fluid past an infinite vertical flat porous surface with ramped wall velocity and temperature, *Int. Commun. Heat Mass Tran.* 126 (2021), 105399.